

Quantifying mobile ions and electronic defects in perovskite-based devices with temperature-dependent capacitance measurements: Frequency vs time domain

Cite as: J. Chem. Phys. 152, 044202 (2020); <https://doi.org/10.1063/1.5132754>

Submitted: 19 October 2019 . Accepted: 09 January 2020 . Published Online: 28 January 2020

Moritz H. Futscher , Mahesh K. Gangishetty , Daniel N. Congreve , and Bruno Ehrler 

COLLECTIONS

Paper published as part of the special topic on [Lead Halide Perovskites](#)

Note: This paper is part of the JCP Special Topic on Lead Halide Perovskites.



View Online



Export Citation



CrossMark

ARTICLES YOU MAY BE INTERESTED IN

[Characterization of perovskite solar cells: Towards a reliable measurement protocol](#)

APL Materials 4, 091901 (2016); <https://doi.org/10.1063/1.4960759>

[The two faces of capacitance: New interpretations for electrical impedance measurements of perovskite solar cells and their relation to hysteresis](#)

Journal of Applied Physics 124, 225702 (2018); <https://doi.org/10.1063/1.5063259>

[Verification and mitigation of ion migration in perovskite solar cells](#)

APL Materials 7, 041111 (2019); <https://doi.org/10.1063/1.5085643>



Lock-in Amplifiers

Zurich Instruments

Watch the Video

Quantifying mobile ions and electronic defects in perovskite-based devices with temperature-dependent capacitance measurements: Frequency vs time domain

Cite as: J. Chem. Phys. 152, 044202 (2020); doi: 10.1063/1.5132754

Submitted: 19 October 2019 • Accepted: 9 January 2020 •

Published Online: 28 January 2020



View Online



Export Citation



CrossMark

Moritz H. Futscher,¹ Mahesh K. Gangishetty,² Daniel N. Congreve,² and Bruno Ehrler^{1,a)}

AFFILIATIONS

¹AMOLF, Center for Nanophotonics, Science Park 104, 1098 XG Amsterdam, The Netherlands

²Rowland Institute at Harvard, 100 Edwin H. Land Blvd., Cambridge, Massachusetts 02142, USA

Note: This paper is part of the JCP Special Topic on Lead Halide Perovskites.

a) Author to whom correspondence should be addressed: ehrlers@amolf.nl

ABSTRACT

Perovskites have proven to be a promising candidate for highly efficient solar cells, light-emitting diodes, and x-ray detectors, overcoming limitations of inorganic semiconductors. However, they are notoriously unstable. The main reason for this instability is the migration of mobile ions through the device during operation as they are mixed ionic–electronic conductors. Here, we show how measuring the capacitance in both the frequency and the time domain can be used to study ionic dynamics within perovskite-based devices, quantifying activation energy, diffusion coefficient, sign of charge, concentration, and the length of the ionic double layer in the vicinity of the interfaces. Measuring the transient of the capacitance furthermore allows for distinguishing between ionic and electronic effects.

© 2020 Author(s). All article content, except where otherwise noted, is licensed under a Creative Commons Attribution (CC BY) license (<http://creativecommons.org/licenses/by/4.0/>). <https://doi.org/10.1063/1.5132754>

INTRODUCTION

Measuring the temperature-dependent capacitance as a function of frequency or time is a well-established technique in experimental physics to quantify electronic defect states in semiconductors.^{1–4} The most famous examples are deep-level transient spectroscopy (DLTS) and thermal admittance spectroscopy (TAS).^{5,6} These techniques allow for quantifying activation energy, attempt-to-escape frequency, sign, and concentration of electronic defect states.

Due to the intriguing properties of perovskites such as high charge-carrier mobilities, long diffusion lengths, strong absorption, and low exciton binding energies, perovskites have been successfully used in many optoelectronic applications including light-emitting diodes, lasers, and x-ray detectors.^{7–10} Both DLTS and TAS have been used to study perovskite-based devices.^{11–15} To measure

electronic defect states, these techniques rely on the depletion approximation, assuming that the depletion region is free of mobile carriers. In the case of perovskites, however, this assumption is not fulfilled because they are mixed ionic–electronic conductors, leaving slow charged carriers (mobile ions) within the depletion region.¹⁶ Consequently, temperature-dependent capacitance measurements may lead to misleading results.¹⁷ If used correctly, measuring the capacitance as a function of frequency or time can be used to quantify these mobile ions within the perovskite bulk.^{18–23}

Here, we review the difference in studying mobile ions by capacitance measurements in the frequency and in the time domain. Based on the example of a $\text{PEABr}_{0.2}\text{Cs}_{0.4}\text{MA}_{0.6}\text{PbBr}_3$ quasi-2D/3D perovskite layer typically used for light-emitting diodes,^{24,25} we show how both measurements can be used to quantify the properties of mobile ions such as activation energy, diffusion coefficient, sign of

charge, concentration, and the length of the ionic double layer. Furthermore, we show how a distinction between mobile ions and electronic defect states can be made when measuring the capacitance in the time domain, allowing both mobile ions and electronic defect states to be quantified.

CAPACITANCE MEASUREMENT

Most optoelectronic devices such as solar cells and light-emitting diodes can be approximated as a parallel-plate device with the active material sandwiched between the two contacts. The capacitance of such a parallel-plate device is given by

$$C = \frac{\epsilon \epsilon_0 A}{w_D}, \quad (1)$$

where ϵ_0 is the vacuum permittivity, A is the active area of the device, and w_D is the depletion layer width, plus a possible additional dielectric contribution of the contact layers. In case of full depletion, w_D corresponds to the thickness of the active layer, i.e., the thickness of the perovskite layer, and the capacitance corresponds to the geometric capacitance of the device C_{geo} . The dielectric permittivity of the material $\epsilon = \epsilon' + i\epsilon''$ is a complex frequency-dependent tensor. To obtain the complex capacitance of the device, we measure the impedance response by applying a time-varying electric field with amplitude V_0 at frequency ω and measuring the current response $I_0 \sin(\omega t + \Phi)$, as indicated in Fig. 1. The impedance Z is defined as

$$Z(t) = \frac{V_0 \sin(\omega t)}{I_0 \sin(\omega t + \Phi)} = Z_0 e^{-i\Phi} = Z' - iZ'', \quad (2)$$

where Φ is the phase delay between the voltage input and the current response and the modulus $Z_0 = V_0/I_0$ is the ratio between the amplitude of the voltage and the current signal. The complex capacitance is given by

$$C^*(\omega) = (i\omega Z)^{-1} = C'(\omega) - iC''(\omega), \quad (3)$$

where C' and C'' are coupled by the Kramers–Kronig relations.²⁶ In semiconductor devices, the measurement of the capacitance thus measures the complex dielectric permittivity of the device.

FREQUENCY VS TIME DOMAIN

In a dielectric material with a Debye relaxation, i.e., a physical process exhibiting an exponential relaxation with a single time

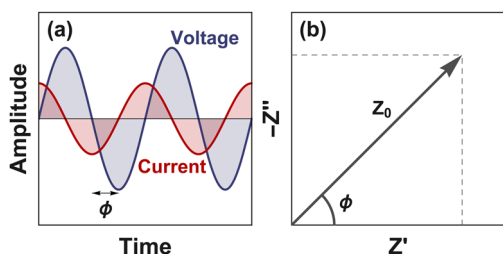


FIG. 1. (a) Impedance measurements are based on applying a sinusoidal voltage with a certain frequency and measuring the current response. (b) Impedance expressed as the modulus Z_0 and the phase angle Φ .

constant τ , the complex dielectric response function is

$$\epsilon(\omega) = \epsilon'(\omega) - i\epsilon''(\omega) = \epsilon_\infty + \frac{\epsilon_s - \epsilon_\infty}{1 + i\omega\tau}, \quad (4)$$

where ϵ_s and ϵ_∞ are the static and asymptotic high frequency values of the dielectric constant, respectively.²⁷ The real part (ϵ') is a measure of the ability to store energy in the dielectric material, and the imaginary part (ϵ'') is a measure of the dielectric loss [see Fig. 2(a)]. In the imaginary part, one can see a distinctive peak at a frequency of $\omega_0 = 1/\tau$, corresponding to the maximum dielectric loss in the material, i.e., the irreversible transfer of energy from the external stimulus to the dielectric material. At lower frequencies, the electrical displacement can follow the applied electric field, whereas at higher frequencies, the material has no time to respond.

Alternatively, one can, instead, measure the transient response of the system following an abrupt change in driving field. Using Laplace transformation to convert Eq. (4) from the frequency domain into the time domain then yields

$$\epsilon(t) = \epsilon_\infty + (\epsilon_s - \epsilon_\infty) \left(1 - \exp\left(-\frac{t}{\tau}\right) \right), \quad (5)$$

which is illustrated in Fig. 2(b). Both the frequency and the time domain contain identical information.

The physical origin of a Debye process leading to the dielectric permittivity shown in Fig. 2 can, for example, be the thermal emission of trapped charge carriers or the migration of mobile ions within the perovskite bulk. The magnitude of $\epsilon_s - \epsilon_\infty$ is then directly related to the number of trapped charge carriers or mobile ions.

In the case of electronic defect states within the bandgap, the kinetics of charge-carrier capture and emission by these defect states can be described in the context of the Shockley–Read–Hall model.^{28,29} In this model, the time constant measured is due to thermal emission of trapped charge carriers (see Sec. 1 in the supplementary material for details). However, the model assumes that the measured time constant results solely from the occupation/emission of electronic defect states. If a significant density of mobile ions is present within the studied material, this analysis may yield misleading results as the migration of mobile ions typically dominates the slow capacitance signal, and it hence cannot be assigned to be solely from electronic defect states.¹⁷

In the following, we show how this dominating signal can be used to study ion migration, both in the frequency domain with impedance spectroscopy and in the time domain with transient ion drift (TID). Finally, we suggest that the time domain can be used to

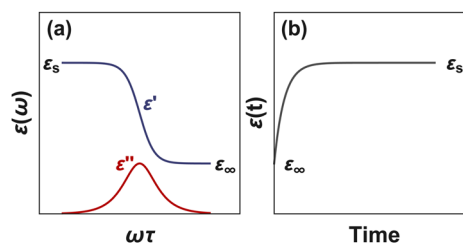


FIG. 2. Debye dielectric material represented in (a) the frequency domain and (b) the time domain after a step function of applied electric field. Both the frequency and the time domain contain identical information.

also measure electronic defect states by suppressing the signal from mobile ions.

IMPEDANCE SPECTROSCOPY

Impedance spectroscopy measures the capacitance as a function of frequency to observe dielectric relaxation in a material as shown in Fig. 2(a). To illustrate the difference between impedance spectroscopy and transient ion drift, we measure a perovskite-based device illustrated in Fig. 3(a) (details of the device are found in Sec. S2 in the supplementary material). We measure the modulus and the phase angle at short circuit in the dark [Fig. 3(b)] to obtain the complex capacitance from Eq. (3). Figure 3(c) shows the real part and Fig. 3(d), the imaginary part of the complex capacitance. At low frequencies, the phase angle is close to -90° , showing that the device operates in a capacitor-like manner. At high frequencies, the contact resistance is dominating the measured impedance response resulting in a decrease in phase angle. The real part of the capacitance shows a plateau at medium frequencies [Fig. 3(c)]. Assuming that the perovskite layer is mostly depleted at short circuit, we obtain a dielectric constant of 7.3 ± 0.1 based on the mean of three measurements, which is in good agreement with the dielectric constant obtained for CsPbBr₃.³⁰ We observe a small increase in the real part of the capacitance C' at low frequencies which is accompanied with a peak in the imaginary part C'' , similar to the dielectric relaxation shown in Fig. 2(a). The peak in the imaginary part shifts to lower frequencies with decreasing temperatures, which corresponds to the presence of a thermally activated process. In perovskite-based devices, such a behavior typically arises from the migration of mobile ions within the perovskite layer.³¹ We hence, assume in the following that the change in capacitance arises from ion migration. Later, we validate this assumption with transient ion drift.

Due to the different work functions of the contacts, the perovskite layer is subject to an internal electric field in optoelectronic devices. This leads to an accumulation of mobile ions at the contact interfaces.³² Mobile ions that accumulated at the contact interfaces form a diffuse ionic double layer that strongly influence the current injection rates of perovskites-based devices under operation.¹⁸ The application of an oscillating voltage with a frequency ω then leads to the migration of mobile ions with a peak in the imaginary part of the complex capacitance with a maximum at the frequency,

$$\omega_0 = 2\pi f_0 = \frac{1}{\tau} = \frac{D}{l^2}, \quad (6)$$

where f is the measured angular frequency and l is the diffusion length. Often, the ion diffusion length is assumed to correspond to the Debye length l_D given by

$$l_D = \sqrt{\frac{\epsilon\epsilon_0 k_B T}{q^2 N}}, \quad (7)$$

where k_B is Boltzmann's constant, T is the temperature, and N is the doping density.³³ The diffusion coefficient can be expressed as^{34,35}

$$D = \frac{v_0 d^2}{6} \exp\left(-\frac{\Delta G}{k_B T}\right) = \frac{v_0 d^2}{6} \exp\left(\frac{\Delta S}{k_B}\right) \exp\left(-\frac{\Delta H}{k_B T}\right), \quad (8)$$

where v_0 is the attempt frequency of an ionic jump and d is the jump distance. ΔG , ΔS , and ΔH are the change in Gibbs free energy, entropy, and enthalpy during the jump of a mobile ion. The activation enthalpy is often referred to as the activation energy E_A . The attempt frequency is the frequency of an attempt to break or loosen a bond, related to the vibration frequency and often assumed to be in the order of 10^{12} s^{-1} .³⁶ Assuming that the attempt frequency is temperature independent, Eq. (8) can be simplified to

$$D = D_0 \exp\left(-\frac{E_A}{k_B T}\right), \quad (9)$$

where D_0 is a temperature-independent pre-factor. Assuming furthermore, that the diffusion of mobile ions is primarily within the Debye layer in the vicinity to the interfaces, Eq. (6) can be written as

$$\tau = \frac{\epsilon_0 \epsilon k_B T}{q^2 N D_0} \exp\left(\frac{E_A}{k_B T}\right). \quad (10)$$

By plotting the measured frequency as a function of temperature in an Arrhenius plot, the activation energy for ion migration can be obtained.

In order to obtain the concentration of mobile ions by impedance spectroscopy measurements, it is often assumed that the excess capacitance at low frequencies is related to the width of the Debye length as³¹

$$\Delta C = \frac{\epsilon\epsilon_0 A}{l_D}. \quad (11)$$

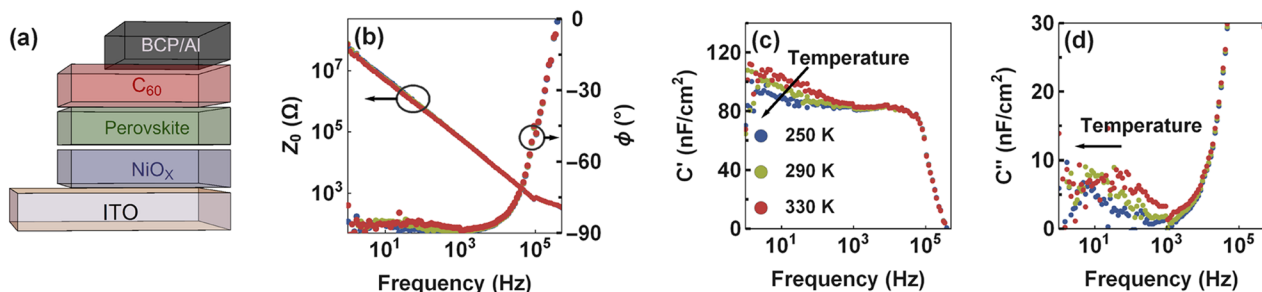


FIG. 3. (a) Schematic representation of the device structure. The perovskite composition is $\text{PEABr}_{0.2}\text{CS}_{0.4}\text{MA}_{0.6}\text{PbBr}_3$. (b) Modulus (Z) and phase angle (Φ) of the perovskite-based device measured at short circuit in the dark together with the corresponding (c) real and (d) imaginary parts of the complex capacitance. The peak in the imaginary part corresponds to the temperature-dependent diffusion of mobile ions within the perovskite. The temperature dependence reveals the activation energy and the pre-factor.

In our case, this would result in a Debye length of 334 ± 20 nm, much larger than the perovskite layer itself. This shows that, in perovskite devices, interfacial effects complicate the quantification of the concentration of mobile ions. Ebadi *et al.* have recently shown that the excess capacity at low frequencies is related to modified electronic charge injection and transport by mobile ions accumulating in the vicinity of the interface and cannot be used to quantify charge accumulation.³⁷

Note that also in the presence of electronic defect states, an increase in capacitance at low frequencies is expected,⁶ which can only be distinguished with impedance measurements from the effect of mobile ions when devices with different perovskite thicknesses are measured.³¹ In addition, the diffusion coefficient can only be obtained if the diffusion length within the perovskite is known. Here, we assumed that the diffusion length is equal to the Debye layer. However, it has also been suggested that the migration of mobile ions extends throughout the perovskite bulk.^{38,39} Furthermore, it was shown that the interfaces play an important role as charge accumulation at interfaces leads to an additional increase in capacitance.^{40–43} Capacitance measurements in the time domain offer the complementary information needed to assign the observed feature to the migration of mobile ions. Only when measuring the transient of the capacitance can the diffusion coefficient be obtained without prior knowledge of the diffusion length. Transient capacitance measurements, furthermore, allow us to distinguish between effects caused by electronic defect states and mobile ions.

TRANSIENT ION DRIFT

Transient ion-drift measurements are based on measuring the capacitance transient after applying a voltage bias.⁴⁴ The voltage is chosen such that it collapses the depletion layer within the perovskite. The depletion layer width within the perovskite is approximated as⁴⁵

$$w_D = \sqrt{\frac{2\epsilon_0\epsilon}{qN}}(V_{bi} - V), \quad (12)$$

where V_{bi} is the built-in potential. The depletion capacitance is directly related to the depletion width as

$$C_{dl} = \epsilon_0\epsilon \frac{A}{w_D} = A\sqrt{\frac{q\epsilon_0\epsilon N}{2(V_{bi} - V)}}. \quad (13)$$

Applying a bias thus decreases the depletion layer width, increasing the measured capacitance [see Fig. 4(a)]. The capacitance of the device is obtained by an equivalent circuit model (see Sec. S3 in the supplementary material for details). At higher voltages, the diffusion capacitance C_d starts to dominate the measured capacitance due to the injection of minority carriers. The diffusion capacitance is given as

$$C_d = \frac{q^2 I A N_e}{k_B T} \exp\left(\frac{qV}{nk_B T}\right), \quad (14)$$

where N_e is the total equilibrium charge density at a given voltage V and n is the diode ideality factor.^{46,47} In the case that the depletion capacitance can clearly be distinguished from the diffusion

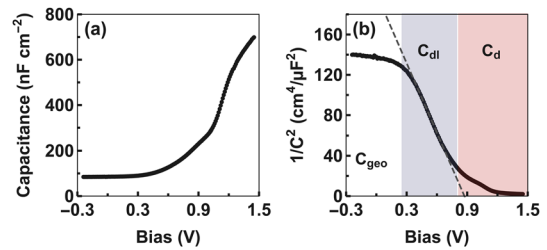


FIG. 4. (a) Capacitance-voltage measurement and (b) Mott-Schottky plot of a perovskite-based device measured at 300 K in the dark at 10 kHz, illustrating different capacitive regimes. Only at a certain voltage regime can the depletion capacitance C_{dl} clearly be identified. At high voltages, the diffusion capacitance C_d starts to dominate the measured capacitance. The linear fit reveals the built-in potential and the doping density. The capacitance was calculated assuming a capacitor in series with a resistor (see Sec. S3 in the supplementary material for details).

capacitance, plotting $C^{-2}(V)$ allows the extraction of the doping density and the built-in potential of the device [see Fig. 4(b)].^{48,49} This is commonly referred to as the Mott-Schottky analysis. We obtain a built-in potential of 0.95 ± 0.05 V and a doping density of $(7 \pm 1) \cdot 10^{17} \text{ cm}^{-3}$, based on the mean of three measurements.

To measure the transient of the capacitance, we apply a bias of 1.25 V, which completely collapses the depletion layer. We note that we are already in the diffusion capacitance regime when applying a 1.25 V bias voltage. However, the initial capacity change caused by the discharge due to the accumulation of minority carriers is much faster than the time resolution of our instrument. The measured capacitance rise and decay are shown in Fig. 5, measured at 10 kHz where the phase angle is close to -90° , such that the measured capacitance is not affected by the series resistance of the device.

Applying a forward bias decreases the depletion width of the device. Mobile ions are now able to diffuse within the perovskite bulk which eventually leads to a uniform ion distribution within the previous depleted region. After removing the bias, the depletion width increases quickly by the movement of electric charge carriers, depleting most of the perovskite bulk according to Eq. (12). Mobile ions within the depleted region will drift toward the interfaces following the internal electric field, changing the depletion width as

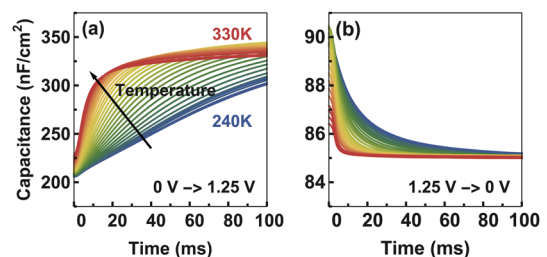


FIG. 5. (a) Capacitance rise and (b) decay of the perovskite-based device measured at 10 kHz where the measured capacitance corresponds to the change in depletion capacitance of the device. The capacitance was calculated assuming a capacitor in parallel with a resistor.

$$w_D(t) = \sqrt{\frac{2\varepsilon_0\varepsilon}{q(N \pm N_{Ion}(t))}}(V_{bi} - V), \quad (15)$$

where $N_{Ion}(t)$ is the density of mobile ions within the depletion region. For ions with the same charge as minority carriers, the sign of the capacitance change is positive, and for ions with the same charge as majority carriers, the sign is negative. The capacitance as a function of time can thus be written as

$$C(t) = C(\infty) \left(1 \pm \frac{N_{Ion}(t)}{N}\right)^{\frac{1}{2}} \approx C(\infty) \left(1 \pm \frac{N_{Ion}(t)}{2N}\right), \quad (16)$$

where $C(\infty)$ is the junction capacitance at the steady state. The approximation is valid as long as the density of the mobile ions is much lower than the doping density. To find $N_{Ion}(t)$, we assume that the thermal diffusion is negligible against drift and solve the drift equation following the work of Heiser *et al.*^{20,44} The temporal evolution of the mobile ions drifting toward the interface can then be described by

$$\frac{\delta N_{Ion}(t)}{\delta t} = -\frac{\delta}{\delta x} N_{Ion}(t) \mu E, \quad (17)$$

where μ is the mobility of mobile ions and E is the electric field in the depletion region. Assuming that the electric field is static and varies linearly within the depletion region as

$$E(x) = E_0 \left(1 - \frac{x}{w_D}\right) \quad (18)$$

and that the drift of mobile ions is not affecting the electric field, we can solve Eq. (17) for $N_{Ion}(t)$. Equation (16) can then be written as

$$C(t) = C(\infty) \pm \Delta C \exp\left(-\frac{t}{\tau}\right), \quad (19)$$

with the time constant τ given by

$$\tau = \frac{w_D}{\mu E}. \quad (20)$$

ΔC is the capacitance change due to the drift of mobile ions toward the interface, directly related to the mobile ion density as

$$\Delta C = C(\infty) - C(0) = C(\infty) \frac{N_{Ion}}{2N}. \quad (21)$$

By expressing the electric field as a function of the doping density as

$$E = \frac{q w_D N}{\varepsilon_0 \varepsilon}, \quad (22)$$

together with the Einstein relation, the time constant can be written as

$$\tau = \frac{k_B T \varepsilon_0 \varepsilon}{q^2 D N}, \quad (23)$$

with the diffusion coefficient given by Eq. (9). This equation can now be used to extract the diffusion coefficient and activation energy from the measured capacitance transients. Note that this equation is the same as Eq. (10), which describes the time constant for ion migration in the frequency domain.

Note that we have assumed a linear electric field within the depletion region and that the electric field is unaffected by the drift of mobile ions, which is only true if the density of mobile ions is small compared to the background doping density. In the case of a mobile ion density close to the background doping density, the screening of the electric field by mobile ions might lead to a non-trivial time dependence of the capacitance transient,²⁰ transient that would have a non-exponential behavior making the analysis more complex. In our devices, the decay is exponential. Furthermore, we did not observe an initial dip in the capacitance transient, sometimes observed in relation to the redistribution of mobile ions inside the depletion region.²⁰ We have further assumed that the total ion concentration is conserved, i.e., mobile ions are not diffusing into the contact layers.

A unique feature of transient ion-drift measurements is that one can differentiate between mobile cations and mobile anions. Here, the negative capacitance change in Fig. 5(b) measures an increase in depletion width due to ions migrating toward the contact interfaces. Under the assumption of a p-type perovskite layer, the negative capacitance change in Fig. 5(b), hence, corresponds to the migration of an anion. We thus attribute the measured changes in capacitance due to bromide migration, presumably due to vacancy-mediated migration.^{50,51}

The Arrhenius plots together with the obtained activation energies for both impedance spectroscopy and transient ion-drift measurements are shown in Fig. 6. For impedance spectroscopy and transient ion-drift measurements, we obtain very similar activation energies of 0.13 ± 0.01 eV and 0.14 ± 0.01 eV, respectively. The obtained activation energy is close to theoretical predictions and experimental observations for the migration of bromide in MAPbBr₃ and CsPbBr₃ (0.09–0.25 eV).^{52–54}

From the capacitance transients, we obtain a concentration of $(5.1 \pm 2.5) \times 10^{16}$ cm⁻³ and a diffusion coefficient of $(3.1 \pm 0.4) \times 10^{-11}$ cm²/s for the mobile anions. We can now use this diffusion coefficient together with the frequency of the dielectric loss peak [Fig. 3(d)] to obtain a diffusion length for ion migration of 6.2 ± 0.4 nm from Eq. (6). The calculated diffusion length is larger than the Debye length of 3.9 ± 0.3 nm calculated from Eq. (7), suggesting that the assumption that the diffusion of mobile ions during frequency-dependent capacitance measurements is limited to the Debye layer is not fulfilled. This underestimation of the diffusion length explains the difference between impedance spectroscopy and transient ion-drift measurements in Fig. 6(a). However, both the

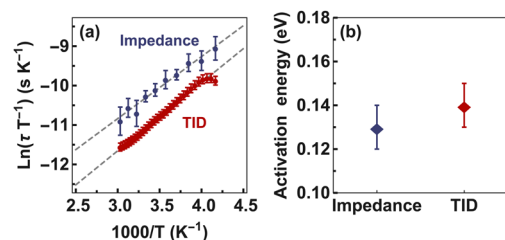
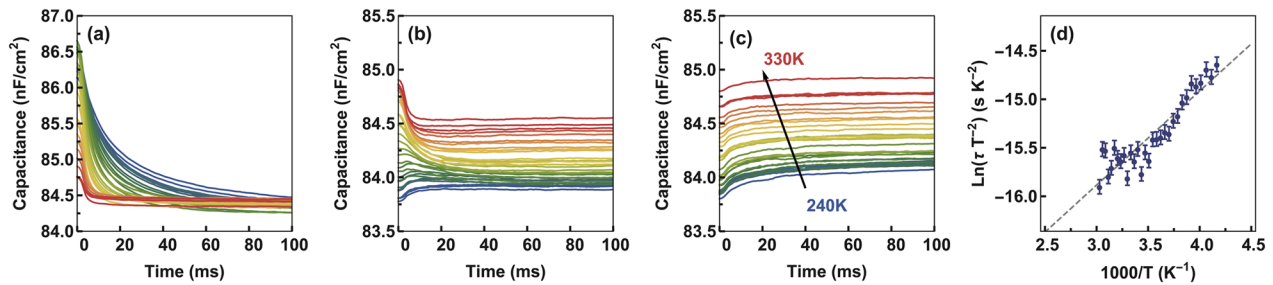


FIG. 6. (a) Arrhenius plot of the measured thermal emission rates by impedance spectroscopy and transient ion drift (TID). (b) Activation energies obtained from the two measurement techniques based on the mean out of three measurements each.

TABLE I. Comparison of rise and decay times of electronic defect states and mobile ions at room temperature assuming a defect state with a trap energy between 0.2 eV and 0.6 eV.

	Electronic defect states	Mobile ions
Rise time	Trapping: $\tau_{trap} = \frac{1}{\sigma v_{th} N_T} \approx 10^{-13} - 10^{-10}$ s	Diffusion: $\tau_{diff} = \frac{w_D^2}{D} \approx 10^{-1} - 10^1$ s
Decay time	De-trapping: $\tau_{detrap} = \frac{1}{\sigma v_{th} N_T} \exp\left(\frac{E_T}{k_B T}\right) \approx 10^{-10} - 10^0$ s	Drift: $\tau_{drift} = \frac{w_D^2 k_B T}{D q V_{bi}} \approx 10^{-3} - 10^0$ s

**FIG. 7.** Capacitance transient measurements between 240 K and 330 K in steps of 3 K measured at 0 V at 10 kHz. Capacitance transients are measured after applying a bias of 1.25 V for (a) 2 s, (b) 20 ms, and (c) 0.2 ms. (d) Arrhenius plot of the thermal emission rates from (c). The linear fit reveals the activation energy and the attempt-to-escape frequency of electronic defect states.

calculation of the diffusion length and the Debye layer thickness depend on the dopant density and the dielectric constant, which are determined experimentally. In addition, there may be a difference in ion migration near the interfaces and through the bulk. In this regard, the obtained results are fairly consistent in both the frequency and the time domain.

ELECTRONIC DEFECT STATES VS MOBILE IONS

Electronic defect states and mobile ions appear very similar in both the frequency and the time domain. To distinguish mobile ions from electronic defect states, the underlying ionic processes have to be understood. Uniquely, transient capacitance measurements can distinguish between ionic and electronic effects as they show different ratios between capacitance rise and decay time. The characteristic rise and decay times for both mobile ions and electronic defect states are shown in Table I. In the case of mobile ions, the voltage pulse is designed to collapse the depletion region. The capacitance rise time [Fig. 5(a)] is, hence, related to the diffusion of mobile ions, i.e., $\tau_{diff} \propto \frac{w_D^2}{D}$. After switching off the voltage, the ions drift back to the interfaces. The decay time of the capacitance [Fig. 5(b)] is, hence, related to the drift of mobile ions, i.e., $\tau_{drift} = \frac{w_D}{\mu E}$, when the electric field is approximated by $E = \frac{V}{w_D}$. Hence, in the case of mobile ions, the ratio between rise and decay time is expected to be larger than 1, i.e., $\tau_{diff}/\tau_{drift} > 1$. The obtained time scales for the capacitance rise and decay in Fig. 5 are shown in Fig. S5.

In contrast, the capture and emission rate for electronic defect states follows from the Shockley–Read–Hall model (see Table I and Sec. 1 in the supplementary material), resulting in a ratio between rise and decay time smaller than 1, i.e., $\frac{\tau_{trap}}{\tau_{detrap}} < 1$. Measuring the rise and the decay of the capacitance, thus, allows us to

distinguish between capacitance changes due to electronic defect states and mobile ions.

The difference in the time scales also allows us to exclusively measure electronic defect states, by using a very short pulse time for the filling voltage. Figure 7 shows measured capacitance transients after a filling voltage of 1.25 V for different pulse durations. Applying a voltage pulse for 2 s allows mobile ions to be measured since mobile ions have sufficient time to diffuse from the interfaces into the perovskite bulk [Fig. 7(a)]. On the other hand, applying a voltage bias for 0.2 ms only fills electronic defect states present in the material as ions do not have enough time to diffuse into the bulk [Fig. 7(c)]. When applying a bias for 20 ms, both ions and electronic defects states are measured [Fig. 7(b)]. The Arrhenius plot of the measured thermal emission rates for electronic defect states is shown in Fig. 7(d). We obtain a trap depth of 0.08 ± 0.01 eV, a concentration of $3 \times 10^{15} \text{ cm}^{-3}$, and an attempt-to-escape frequency of $(1.3 \pm 0.4) 10^{13} \text{ s}^{-1}$. The obtained concentration of electronic defect states is much lower than the concentration of mobile ions. We therefore assume that the presence of electronic defect states is not influencing our measurements of mobile ions.

CONCLUSION

Capacitance techniques must be applied with caution to mixed ionic–electronic conductors because the measured capacitance features can be caused by both mobile ions and electronic defect states. We have compared conventional impedance spectroscopy to capacitance transient measurements and have shown that transient measurements have the virtue that a distinction between electronic defect states and mobile ions can be made. In addition, transient ion drift allows fast and non-destructive quantification of activation energy, diffusion coefficient, sign of charge, and

concentration of mobile ions in perovskite-based devices. Using the diffusion coefficient obtained by transient ion drift, the length of the ionic double layer can be determined from impedance spectroscopy measurements. We have also shown that transient capacitance measurements can be used to quantify electronic defect states in perovskite-based devices when ionic processes are understood.

Since the migration of mobile ions is a key degradation mechanism in perovskite-based devices, reducing ion migration is crucial for the fabrication of stable devices. Capacitance techniques provide a tool to systematically investigate the effects of different passivation agents, fabrication methods, and perovskite compositions on ion migration in full perovskite-based devices guiding the way to long-lasting devices, critical for commercialization.

SUPPLEMENTARY MATERIAL

See the [supplementary material](#) for further information on the Shockley–Read–Hall model, experimental details, current-voltage characteristics, the choice of the equivalent circuit model, and temperature-dependent rise and decay times.

ACKNOWLEDGMENTS

The authors thank Esther Alarcón Lladó for carefully reading and commenting on the manuscript. The work of M.H.F. and B.E. is part of the Dutch Research Council (NWO) and was performed at the research institute AMOLF. D.N.C. and M.K.G. acknowledge the support of the Rowland Fellowship at the Rowland Institute at Harvard University.

REFERENCES

- G. L. Miller, D. V. Lang, and L. C. Kimerling, *Annu. Rev. Mater. Sci.* **7**, 377 (1977).
- J. Heath and P. Zabierowski, *Advanced Characterization Techniques for Thin Film Solar Cells* (Wiley-VCH Verlag GmbH & Co. KGaA, Weinheim, Germany, 2016), pp. 93–119.
- J. V. Li and G. Ferrari, *Capacitance Spectroscopy of Semiconductors* (Jenny Stanford Publishing, 2018).
- E. von Hauff, *J. Phys. Chem. C* **123**, 11329 (2019).
- D. V. Lang, *J. Appl. Phys.* **45**, 3023 (1974).
- T. Walter, R. Herberholz, C. Müller, and H. W. Schock, *J. Appl. Phys.* **80**, 4411 (1996).
- A. Miyata, A. Mitioglu, P. Plochocka, O. Portugall, J. T. W. Wang, S. D. Stranks, H. J. Snaith, and R. J. Nicholas, *Nat. Phys.* **11**, 582 (2015).
- D. Shi, V. Adinolfi, R. Comin, M. J. Yuan, E. Alarous, A. Buin, Y. Chen, S. Hoogland, A. Rothenberger, K. Katsiev, Y. Losovyj, X. Zhang, P. A. Dowben, O. F. Mohammed, E. H. Sargent, and O. M. Bakr, *Science* **347**, 519 (2015).
- S. Yakunin, M. Sytnyk, D. Krieger, S. Shrestha, M. Richter, G. J. Matt, H. Azimi, C. J. Brabec, J. Stangl, M. V. Kovalenko, and W. Heiss, *Nat. Photonics* **9**, 444 (2015).
- S. D. Stranks and H. J. Snaith, *Nat. Nanotechnol.* **10**, 391 (2015).
- Y. Zhao, H. Tan, H. Yuan, Z. Yang, J. Z. Fan, J. Kim, O. Voznyy, X. Gong, L. N. Quan, C. S. Tan, J. Hofkens, D. Yu, Q. Zhao, and E. H. Sargent, *Nat. Commun.* **9**, 1607 (2018).
- Y. Chen, N. Li, L. Wang, L. Li, Z. Xu, H. Jiao, P. Liu, C. Zhu, H. Zai, M. Sun, W. Zou, S. Zhang, G. Xing, X. Liu, J. Wang, D. Li, B. Huang, Q. Chen, and H. Zhou, *Nat. Commun.* **10**, 1112 (2019).
- S. Heo, J. Lee, J.-B. Park, K. Kim, D.-J. Yun, Y. S. Kim, J. K. Shin, G. Seo, T. K. Ahn, Y. Lee, M. K. Nazeeruddin, D. Lee, M. Seol, J. Lee, J.-B. Park, K. Kim, D.-J. Yun, Y. S. Kim, J. K. Shin, T. K. Ahn, and M. K. Nazeeruddin, *Energy Environ. Sci.* **10**, 1128 (2017).
- J. W. Rosenberg, M. J. Legodi, Y. Rakita, D. Cahen, and M. Diale, *J. Appl. Phys.* **122**, 145701 (2017).
- A. Y. Polyakov, N. B. Smirnov, I. V. Shchemerov, D. S. Saranin, T. S. Le, S. I. Didenko, D. V. Kuznetsov, A. Agresti, S. Pescetelli, F. Matteocci, and A. Di Carlo, *Appl. Phys. Lett.* **113**, 263501 (2018).
- J. M. Frost and A. Walsh, *Acc. Chem. Res.* **49**, 528 (2016).
- O. Almora, M. Garcia-Battle, and G. Garcia-Belmonte, *J. Phys. Chem. Lett.* **10**, 3661 (2019).
- H. Wang, A. Guerrero, A. Bou, A. M. Al-Mayouf, and J. Bisquert, *Energy Environ. Sci.* **12**, 2054 (2019).
- M. H. Futscher, J. M. Lee, L. McGovern, L. A. Muscarella, T. Wang, M. I. Haider, A. Fakharuddin, L. Schmidt-Mende, and B. Ehrler, *Mater. Horizons* **6**, 1497 (2019).
- T. Heiser and E. Weber, *Phys. Rev. B* **58**, 3893 (1998).
- P. Lopez-Varo, J. A. Jiménez-Tejada, M. Garcia-Rosell, S. Ravishankar, G. Garcia-Belmonte, J. Bisquert, and O. Almora, *Adv. Energy Mater.* **8**, 1702772 (2018).
- A. Pockett, G. E. Eperon, N. Sakai, H. J. Snaith, L. M. Peter, and P. J. Cameron, *Phys. Chem. Chem. Phys.* **19**, 5959 (2017).
- S. Reichert, J. Flemming, Q. An, Y. Vaynzof, J.-F. Pietschmann, and C. Deibel, *Phys. Rev. Applied* (to be published) (2019).
- M. K. Gangishetty, S. N. Sanders, and D. N. Congreve, *ACS Photonics* **6**, 1111 (2019).
- S. Hou, M. K. Gangishetty, Q. Quan, and D. N. Congreve, *Joule* **2**, 2421 (2018).
- R. de L. Kronig, *J. Opt. Soc. Am.* **12**, 547 (1926).
- P. Debye, *Trans. Faraday Soc.* **30**, 679 (1934).
- W. Shockley and W. T. Read, *Phys. Rev.* **87**, 835 (1952).
- R. N. Hall, *Phys. Rev.* **87**, 387 (1952).
- Z. Yang, A. Surrente, K. Galkowski, A. Miyata, O. Portugall, R. J. Sutton, A. A. Haghighirad, H. J. Snaith, D. K. Maude, P. Plochocka, and R. J. Nicholas, *ACS Energy Lett.* **2**, 1621 (2017).
- O. Almora, I. Zarazua, E. Mas-Marza, I. Mora-Sero, J. Bisquert, and G. Garcia-Belmonte, *J. Phys. Chem. Lett.* **6**, 1645 (2015).
- J. Bisquert, G. Garcia-Belmonte, and A. Guerrero, *Organic-Inorganic Halide Perovskite Photovoltaics: From Fundamentals to Device Architectures* (Springer International Publishing, Cham, 2016), pp. 163–199.
- E. Hückel, *Ergebnisse der exakten Naturwissenschaften* (Springer Berlin Heidelberg, Berlin, Heidelberg, 1924), pp. 199–276.
- G. H. Vineyard, *J. Phys. Chem. Solids* **3**, 121 (1957).
- D. Meggiolaro, E. Mosconi, and F. De Angelis, *ACS Energy Lett.* **4**, 779 (2019).
- J. Koettgen, T. Zacherle, S. Grieshammer, and M. Martin, *Phys. Chem. Chem. Phys.* **19**, 9957 (2017).
- F. Ebadi, N. Taghavinia, R. Mohammadpour, A. Hagfeldt, and W. Tress, *Nat. Commun.* **10**, 1574 (2019).
- W. Peng, C. Aranda, O. M. Bakr, G. Garcia-Belmonte, J. Bisquert, and A. Guerrero, *ACS Energy Lett.* **3**, 1477 (2018).
- M. Bag, L. A. Renna, R. Y. Adhikari, S. Karak, F. Liu, P. M. Lahti, T. P. Russell, M. T. Tuominen, and D. Venkataraman, *J. Am. Chem. Soc.* **137**, 13130 (2015).
- H.-S. Kim, I.-H. Jang, N. Ahn, M. Choi, A. Guerrero, J. Bisquert, and N.-G. Park, *J. Phys. Chem. Lett.* **6**, 4633 (2015).
- I. Zarazua, G. Han, P. P. Boix, S. Mhaisalkar, F. Fabregat-Santiago, I. Mora-Seró, J. Bisquert, and G. Garcia-Belmonte, *J. Phys. Chem. Lett.* **7**, 5105 (2016).
- A. Guerrero, G. Garcia-Belmonte, I. Mora-Sero, J. Bisquert, Y. S. Kang, T. J. Jacobsson, J.-P. Correa-Baena, and A. Hagfeldt, *J. Phys. Chem. C* **120**, 8023 (2016).
- S. A. L. Weber, I. M. Hermes, S.-H. Turren-Cruz, C. Gort, V. W. Bergmann, L. Gilson, A. Hagfeldt, M. Graetzel, W. Tress, and R. Berger, *Energy Environ. Sci.* **11**, 2404 (2018).
- T. Heiser and A. Mesli, *Appl. Phys. A: Solids Surf.* **57**, 325 (1993).

- ⁴⁵S. M. Sze and K. K. Ng, *Physics of Semiconductor Devices* (John Wiley & Sons, Inc., 2014).
- ⁴⁶J. Bisquert, *Phys. Chem. Chem. Phys.* **5**, 5360 (2003).
- ⁴⁷S. K. Sharma, D. Pavithra, G. Sivakumar, N. Srinivasamurthy, and B. L. Agrawal, *Sol. Energy Mater. Sol. Cells* **26**, 169 (1992).
- ⁴⁸O. Almora, C. Aranda, E. Mas-Marzá, and G. Garcia-Belmonte, *Appl. Phys. Lett.* **109**, 173903 (2016).
- ⁴⁹M. Fischer, K. Tvingstedt, A. Baumann, and V. Dyakonov, *ACS Appl. Energy Mater.* **1**, 10 (2018).
- ⁵⁰Y. Luo, P. Khoram, S. Brittman, Z. Zhu, B. Lai, S. P. Ong, E. C. Garnett, and D. P. Fenning, *Adv. Mater.* **29**, 1703451 (2017).
- ⁵¹A. Senocrate, I. Moudrakovski, G. Y. Kim, T.-Y. Yang, G. Gregori, M. Grätzel, and J. Maier, *Angew. Chem., Int. Ed.* **56**, 7755 (2017).
- ⁵²J. M. Azpiroz, E. Mosconi, J. Bisquert, and F. De Angelis, *Energy Environ. Sci.* **8**, 2118 (2015).
- ⁵³J. Mizusaki, K. Arai, and K. Fueki, *Solid State Ionics* **11**, 203 (1983).
- ⁵⁴H. Cho, C. Wolf, J. S. Kim, H. J. Yun, J. S. Bae, H. Kim, J. M. Heo, S. Ahn, and T. W. Lee, *Adv. Mater.* **29**, 1700579 (2017).